DOI: 10.1002/chem.201600330

Communication

A Breathing Zirconium Metal-Organic Framework with Reversible Loss of Crystallinity by Correlated Nanodomain Formation

Bart Bueken,[a] Dr. Frederik Vermoortele,[a] Dr. Matthew J. Cliffe,[b] Dr. Michael T. Wharmby,[c,d] Damien Foucher,[e] Jelle Wieme,[f] Dr. Louis Vanduyfhuys,[f] Dr. Charlotte Martineau,[e] Prof. Dr. Norbert Stock,[c] Prof. Dr. Francis Taulelle,[e] Prof. Dr. Veronique Van Speybroeck,[f] Prof. Dr. Andrew L. Goodwin,[b] and Prof. Dr. Dirk De Vos*[a]

[a] Centre for Surface Chemistry and Catalysis, KULeuven
Celestijnenlaan 200F, p. o. box 2461, 3001 Leuven (Belgium)
E-mail: dirk.devos@biw.kuleuven.be

[b] Inorganic Chemistry Laboratory, University of Oxford
South Park Road, Oxford, OX1 3QR (UK)

[c] Institut für Anorganische Chemie, CAU Kiel
Max-Eyth-Strasse 2, 24118 Kiel (Germany)

[d] Diamond Light Source, Harwell Science & Innovation Campus
Didcot, OX11 0DE (UK)

[e] Institut Lavoisier, UMR CNRS 8180
Université de Versailles St-Quentin-en-Yvelines
Avenue des Etats-Unis 45, 78035, Versailles (France)

[f] Center for Molecular Modeling, Ghent University
Technologiepark 903, 9052 Zwijnaarde (Belgium)

Supporting information for this article is available on the WWW under
http://dx.doi.org/10.1002/chem.201600330.

Camouflaged from diffraction: The aliphatic isoreticular analogue of the well-known MOF UiO-66(Zr) undergoes a unique and reversible phase change upon guest removal. This change

involves a topology-dictated loss of long-range order through the correlated formation of short-range ordered nanodomains.

An analogue of UiO-66(Zr) undergoes a reversible #PhaseChange upon guest removal #MOFs

---

Metal-Organic Frameworks

---

dynamic	porosity
metal-organic	frameworks
phase	transitions
structure	elucidation
zirconium	

The isoreticular analogue of the metal-organic framework UiO-66(Zr), synthesized with the flexible *trans*-1,4-cyclohexanedicarboxylic acid as linker, shows a peculiar breathing behavior by reversibly losing long-range crystalline order upon evacuation. The underlying flexibility is attributed to a concerted conformational contraction of up to two thirds of the linkers, which breaks the local lattice symmetry. X-ray scattering data are described well by a nanodomain model in which differently oriented tetragonal-type distortions propagate over about 7-10 unit cells.

The field of metal-organic frameworks (MOFs) has greatly matured over the past decade, with many developing applications.[1-5] Among MOFs, the zirconium carboxylates stand out for their high thermal and chemical stability,[6] but also because, except for a few cases,[7-10] they all share a similar chemistry based on the $[Zr_6O_4(OH)_4(CO_2)_{12}]$ inorganic node.[11, 12] This allows for a rational synthesis of certain topologies by selecting the appropriate, often rigid aromatic linkers.[13] The resulting materials feature tunable but static permanent porosity.

One property that remains surprisingly elusive to realize in Zr-MOFs is a dynamic, stimulus-dependent porosity. Such materials, also called breathing or third-generation MOFs, reversibly undergo a phase change in response to pressure, temperature, or selective guest adsorption, and are considered ideal candidates for sensing or separations.[14-18]

Flexibility in MOFs often originates at the connection between linker and inorganic node. With rigid carboxylates, a typical mechanism is the so-called knee-cap, or linker rotation around the axis through the coordinating oxygen atoms.[18] Zr-MOFs however are not predisposed to be flexible in this way owing to their often high connectivity and the presence of odd-numbered cycles in many topologies. One way to circumvent these issues is to shift flexibility to the linkers.[14-16] Recently Farha *et al*.[19] employed this strategy by using large tetrapodal linkers with bendable arms to synthesize breathing Zr-MOFs.

Flexible, aliphatic linkers could both circumvent the topological constraints on breathing related to their rigid counterparts and enable a guest-selective uptake. However, the only aliphatic Zr-MOFs reported to date, based on adipate, irreversibly collapse upon evacuation, ruling out any breathing.[20]

Herein, we present the synthesis of a flexible Zr-MOF by employing *trans*-1,4-cyclohexanedicarboxylic acid (H_2cdc) as linker. We successfully synthesized ZrCDC, an aliphatic analogue of the widely studied Zr-terephthalate UiO-66 ($[Zr_6O_4(OH)_4(C_8H_4O_4)_6]$).[12] ZrCDC displays a unique breathing behavior with a loss of long-range order in the transition from a cubic, adsorbate-filled form to a lower-symmetry evacuated phase.

As-prepared ZrCDC shows excellent crystallinity (Supporting Information, Figures S1, S2), which is retained upon solvent exchange of DMF occupying the pores for ethanol or water. The structure of ZrCDC was solved by Rietveld refinement of a model derived from the UiO-66 framework against a high-resolution X-ray diffraction pattern collected from a water-exchanged sample (Supporting Information, Figure S3, Table S3).

ZrCDC ($[Zr_6O_4(OH)_4(C_8H_{10}O_4)_6]$) is an isostructural analogue of UiO-66, and consists of hexanuclear Zr-clusters (Figure 1 a), which are bound to twelve neighboring clusters through the ditopic *trans*-1,4-cyclohexanedicarboxylate (cdc^{2-}) linkers. The clusters organize in an **fcu** topology, creating a porous framework with tetrahedral and octahedral cages (Figure 1 b-d) of approximately 4.4 Å and 10.1 Å in diameter.

Although ZrCDC only decomposes at temperatures above 275 °C (Supporting Information, Figure S5), guest removal, even by evaporation at room temperature, results in the disappearance of clearly defined Bragg reflections in the X-ray powder diffraction pattern

of ZrCDC (Figure 2). This loss of long-range crystalline order is also accompanied by a collapse of the ZrCDC pore volume (Supporting Information, Figure S6). However, the persistence of broad diffraction features at low angles hints at an enduring short-range order within the material. Moreover, immersion of the evacuated powder in ethanol or water results in the complete recovery of the crystalline lattice. Counter-intuitively, apolar solvents such as hexane are unable to induce pore opening, despite the hydrophobic nature of the linkers, which points to a guest-specific breathing behavior (Supporting Information, Figure S7). Understanding this reversible desorption-induced amorphization clearly requires insight into the nature of the collapsed phase, hereafter denoted $ZrCDC_{cp}$. Therefore, the latter was investigated by a combination of X-ray total scattering, solid-state ^{13}C magic angle spinning (MAS) NMR and molecular modeling.

Since the breathing may involve conformational changes of the cdc^{2-} linker, these were probed by ^{13}C MAS NMR (Figure 3). In accordance with their Rietveld refined structure, water- and ethanol-exchanged ZrCDC only contain cdc^{2-} in its elongated *e*,*e*-conformation, denoted *e*, (182.0, 45.8 and 29.0 ppm), with the carboxylates occupying equatorial positions. In the $ZrCDC_{cp}$ spectrum however, additional resonances are found, which were assigned to the *a*,*a*-conformation, denoted *a*, of cdc^{2-} by DFT calculations (183.1, 41.5 and 24.3 ppm; Supporting Information, Table S5). Integration of the $ZrCDC_{cp}$ spectrum yields a maximum *a*:*e* ratio of 2:1, indicating a conformational change of 66 % of the linkers from *e* to *a* upon guest removal (Figure 3). Some ethanol (57.8, 18.1 ppm) can still be seen in the $ZrCDC_{cp}$ spectrum, indicating that full guest removal from the framework is not required to elicit the observed structural and conformational changes. A similar situation is encountered in CAU-13 ([Al(OH)(cdc)]) and COK-69 ($[Ti_3O(O)_2(cdc)_3]$). These materials feature crystalline narrow and large pore forms, with ring inversion of half of the linkers governing the transition between these states.[21-23]

The question remains as to why this linker contraction in ZrCDC seems to destroy the crystalline long-range order of the framework. Still, the diffraction pattern of $ZrCDC_{cp}$ indicates that some order on short length scales is preserved. Therefore, an atomic pair distribution function (PDF) analysis was performed for both water-exchanged ZrCDC and

$ZrCDC_{cp}$ to investigate their local structure (Figure 2 b). Both PDFs are dominated by Zr-Zr pairs, since these are the heaviest scatterers (Figure 2 c). Up to 8 Å, the PDF of $ZrCDC_{cp}$ is essentially the same as that of ZrCDC. The loss of crystal symmetry makes robust determination of sample density and absorption parameters difficult, which accounts for the slight mismatch in peak intensities at low *r*. Nevertheless both patterns consist of three sharp peaks belonging to intracluster distances, confirming the integrity of the hexanuclear cluster upon evacuation. Between 8 Å and 18 Å, peaks corresponding to Zr-Zr pairs in adjacent clusters are observed in both PDFs. For $ZrCDC_{cp}$, these peaks broaden and lose intensity with increasing interatomic distances, indicating that the distances between neighboring clusters are less sharply defined than in ZrCDC, but have not changed drastically. This is consistent with the rather small change in linker length upon ring inversion (ca. 0.9 Å), and the fact that at least 33 % of the linkers retain their original *e*-conformation. Beyond 18 Å, only two broad peaks at 25 Å and 36 Å are present for $ZrCDC_{cp}$, which indicates weak ordering beyond the nearest-neighbor cluster shell.

Closer inspection of the $ZrCDC_{cp}$ diffraction pattern reveals three broad reflections (Figure 2 a). In the same range, ZrCDC shows two reflections, (111) and (200). Comparing both sets of reflections reveals a distortion of the ZrCDC face-centered cubic unit cell to a lower-symmetry cell upon drying. A satisfactory Pawley fit of the $ZrCDC_{cp}$ diffraction pattern was obtained in the tetragonal *I*4/*mmm* space group, which is the highest-symmetry subgroup of the parent *Fm*-3*m* space group for which we could obtain a good fit to data (Figure 4 c). Following contraction to a body-centered tetragonal cell (Figure S10), the cubic (111) reflection (d=12.0 Å) is conserved as the (011) reflection (d=11.7 Å). The (200) reflection (d=10.4 Å) however has split into the tetragonal (11-0) and (110) (d=10.6 Å) and (002) (d=8.9 Å) reflections. A similar splitting of the (200) reflection has previously been reported for a tetragonal variant of UiO-66-NH_2.[24] Furthermore, the intensity ratios in the diffraction pattern suggest that the distances between the cubic {001} planes have shortened by approximately 3 Å in $ZrCDC_{cp}$. Geometrically, this would correspond to a contraction of two thirds of the linkers from *e* to *a* along the [001] direction, in accordance with the observed *a*:*e* ratio by NMR spectroscopy. Combining all our observations, we geometrically constructed a tetragonally distorted model for $ZrCDC_{cp}$ (Figure 4 a; Supporting Information, Figures S11-

S13), which maintains the topology and connectivity of ZrCDC: each cluster now connects to twelve neighbors via four *e*-linkers in the (002) plane and eight contracted *a*-linkers above and below this plane.

To correctly fit the broad reflections in the $ZrCDC_{cp}$ powder pattern, a Lorentzian size broadening term was introduced, from which a crystalline domain size of approximately 13.4(1.3) nm or 7-10 tetragonal unit cells was deduced. This domain formation originates from the fact that the ZrCDC cubic unit cell can contract along the three equivalent <100> directions to end up in the correct tetragonal cell. While the direction along which one cell contracts is correlated to the direction selected by its neighbors, the contraction does not propagate through the whole crystal in the same direction. Rather, randomly oriented correlated nanodomains are formed in which short-range order is preserved, with a concomitant loss of the long-range crystalline order of ZrCDC. This behavior was simulated as a cluster growth model (Figure 4 b),[25] which yields a calculated diffraction pattern that reproduces the key features of the $ZrCDC_{cp}$ experimental pattern (Figure 4 c). The tetragonal model represents the limiting case for a 2:1 *a*:*e* ratio. Lower ratios might be accommodated by alternative types of symmetry lowering (for example a rhombohedral-type distortion would correspond to a 1:1 *a*:*e* ratio; Supporting Information, Figure S14). While the tetragonal case clearly dominates based on the form of the diffraction profile and the observed linker ratio, it is possible that both cases could be present in $ZrCDC_{cp}$, for instance at domain boundaries, resulting in intermediate linker ratios.

To obtain more insight in the relative stability of ZrCDC and $ZrCDC_{cp}$, periodic DFT calculations were performed. $ZrCDC_{cp}$ is 102 kJ mol^{-1} per cluster more stable than a hypothetical, open-pore ZrCDC framework owing to a much larger contribution of stabilizing dispersion interactions in $ZrCDC_{cp}$ (Supporting Information, Figure S15). To obtain some insight in the dynamic behavior of ZrCDC and the effect of water adsorption, energies were calculated for the open-pore ZrCDC with a water molecule adsorbed on top of each Zr^{4+} atom, as observed in the Rietveld refinement (Figure 1 a). Each water molecule realizes an energy gain of 38 kJ mol^{-1} by hydrogen bonding to the carboxylates, which indicates that sufficient loading with water could stabilize the open-pore ZrCDC. The hydrophilic nature of

the cluster thus likely dominates the breathing behavior, explaining preferential adsorption for $ZrCDC_{cp}$ of hydrogen-bond-donating molecules such as water or ethanol. Interactions between guests and the cluster μ_3-OH groups could also contribute to this selective uptake.

In summary, we synthesized a breathing analogue of the topologically rigid UiO-66 by using cdc^{2-} as flexible linker. Guest removal results in a tetragonal-type contraction of the crystalline cubic ZrCDC structure, which is accompanied by a loss of long-range order owing to the clustering of these tetragonal cells in differently oriented nanodomains. The breathing of ZrCDC is driven by a selective uptake of hydrogen bond donating molecules, which opens opportunities for its use in separations or sensing applications.

Acknowledgements

B.B., J.W., L.V., V.V.S., and D.D.V. acknowledge the FWO Flanders, KULeuven (Methusalem grant CASAS and IAP 7/05 Functional Supramolecular Systems), the IWT (SBO-project MOFShape), Ghent University, and the ERC (grant 647755) for financial support. M.J.C. and A.L.G. acknowledge the ERC (grant 279705). M.T.W. and N.S. thank the DFG (SPP 1362) and the EU (FP7/2007-2013, grant 228862) for financial support. Parts of this research were carried out at the light source PETRA III at DESY, a member of the Helmholtz Association (HGF). We thank Dr. U. Ruett and O. Gutowski for assistance in using beamline P07.

1. J.-R. Li, R. J. Kuppler, H.-C. Zhou, *Chem. Soc. Rev.* **2009**, *38*, 1477.

2. L. E. Kreno, K. Leong, O. K. Farha, M. Allendorf, R. P. Van Duyne, J. T. Hupp, *Chem. Rev.* **2012**, *112*, 1105.

3. H. Furukawa, K. E. Cordova, M. O'Keeffe, O. M. Yaghi, *Science* **2013**, *341*, 1230444.

4. J. Liu, L. Chen, H. Cui, J. Zhang, L. Zhang, C.-Y. Su, *Chem. Soc. Rev.* **2014**, *43*, 6011.

5. B. Van De Voorde, B. Bueken, J. Denayer, D. De Vos, *Chem. Soc. Rev.* **2014**, *43*, 5766.

6. T. Devic, C. Serre, *Chem. Soc. Rev.* **2014**, *43*, 6097.

7. V. Guillerm, F. Ragon, M. Dan-Hardi, T. Devic, M. Vishnuvarthan, B. Campo, A. Vimont, G. Clet, Q. Yang, G. Maurin, *Angew. Chem. Int. Ed.* **2012**, *51*, 9267; *Angew. Chem.* **2012**, *124*, 9401.

8. D. Feng, H.-L. Jiang, Y.-P. Chen, Z.-Y. Gu, Z. Wei, H.-C. Zhou, *Inorg. Chem.* **2013**, *52*, 12661.

9. L. Cooper, N. Guillou, C. Martineau, E. Elkaim, F. Taulelle, C. Serre, T. Devic, *Eur. J. Inorg. Chem.* **2014**, 6281.

10. G. Mouchaham, L. Cooper, N. Guillou, C. Martineau, E. Elkaïm, S. Bourrelly, P. L. Llewellyn, C. Allain, G. Clavier, C. Serre, *Angew. Chem.* **2015**, *127*, 13495.

11. G. Kickelbick, U. Schubert, *Chem. Ber.* **1997**, *130*, 473.

12. J. H. Cavka, S. Jakobsen, U. Olsbye, N. Guillou, C. Lamberti, S. Bordiga, K. P. Lillerud, *J. Am. Chem. Soc.* **2008**, *130*, 13850.

13. H. Furukawa, F. Gándara, Y.-B. Zhang, J. Jiang, W. L. Queen, M. R. Hudson, O. M. Yaghi, *J. Am. Chem. Soc.* **2014**, *136*, 4369.

14. S. Kitagawa, R. Kitaura, S. Noro, *Angew. Chem. Int. Ed.* **2004**, *43*, 2334; *Angew. Chem.* **2004**, *116*, 2388.

15. Z.-J. Lin, J. Lü, M. Hong, R. Cao, *Chem. Soc. Rev.* **2014**, *43*, 5867.

16. A. Schneemann, V. Bon, I. Schwedler, I. Senkovska, S. Kaskel, R. A. Fischer, *Chem. Soc. Rev.* **2014**, *43*, 6062.

17. S. Horike, S. Shimomura, S. Kitagawa, *Nat. Chem.* **2009**, *1*, 695.

18. G. Férey, C. Serre, *Chem. Soc. Rev.* **2009**, *38*, 1380.

19. P. Deria, D. A. Gomez-Gualdron, W. Bury, H. T. Schaef, T. C. Wang, P. K. Thallapally, A. A. Sarjeant, R. Q. Snurr, J. T. Hupp, O. K. Farha, *J. Am. Chem. Soc.* **2015**, *137*, 13183.

20. H. Reinsch, I. Stassen, B. Bueken, A. Lieb, R. Ameloot, D. De Vos, *CrystEngComm* **2015**, *17*, 331.

21. F. Niekiel, M. Ackermann, P. Guerrier, A. Rothkirch, N. Stock, *Inorg. Chem.* **2013**, *52*, 8699.

22. B. Bueken, F. Vermoortele, D. E. P. Vanpoucke, H. Reinsch, C.-C. Tsou, P. Valvekens, T. De Baerdemaeker, R. Ameloot, C. E. A. Kirschhock, V. Van Speybroeck, *Angew. Chem.* **2015**, *127*, 14118.

23. F. Niekiel, J. Lannoeye, H. Reinsch, A. S. Munn, A. Heerwig, I. Zizak, S. Kaskel, R. I. Walton, D. De Vos, P. Llewellyn, *Inorg. Chem.* **2014**, *53*, 4610.

24. H. Reinsch, B. Bueken, F. Vermoortele, I. Stassen, A. Lieb, K.-P. Lillerud, D. De Vos, *CrystEngComm* **2015**, *17*, 4070.

25. M. J. Cliffe, W. Wan, X. Zou, P. A. Chater, A. K. Kleppe, M. G. Tucker, H. Wilhelm, N. P. Funnell, F.-X. Coudert, A. L. Goodwin, *Nat. Commun.* **2014**, *5*, 4176.

Received: January 25, 2016

Published online on <?><?>

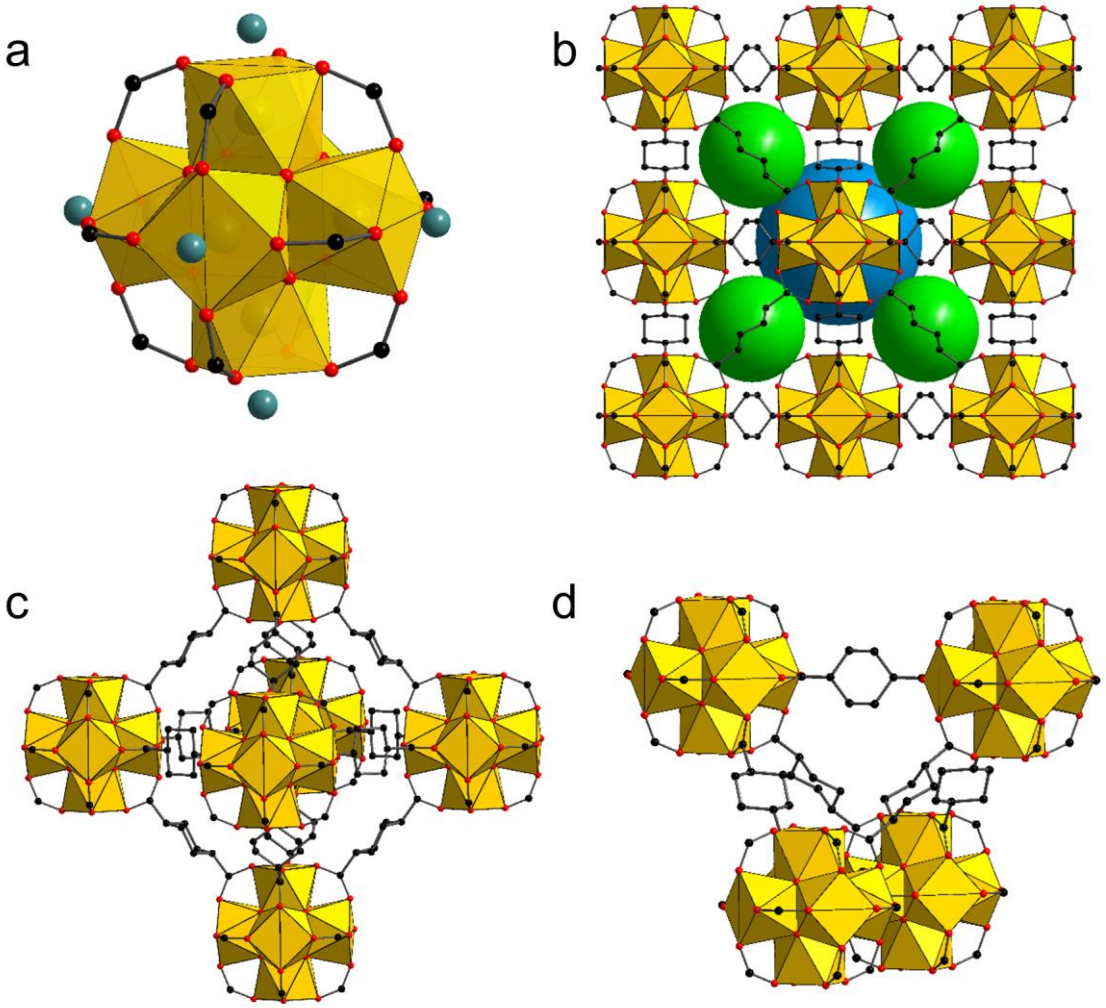

Figure 1 Structure of ZrCDC. $[Zr_6O_4(OH)_4(CO_2)_{12}]$ clusters (a) arrange in an **fcu** topology (b), containing octahedral (b, blue; c) and tetrahedral (b, green; d) cages. Guests have been omitted. The water sorption site in (a) indicated in light blue. O red, C black, Zr yellow. Guests and H-atoms omitted for clarity.

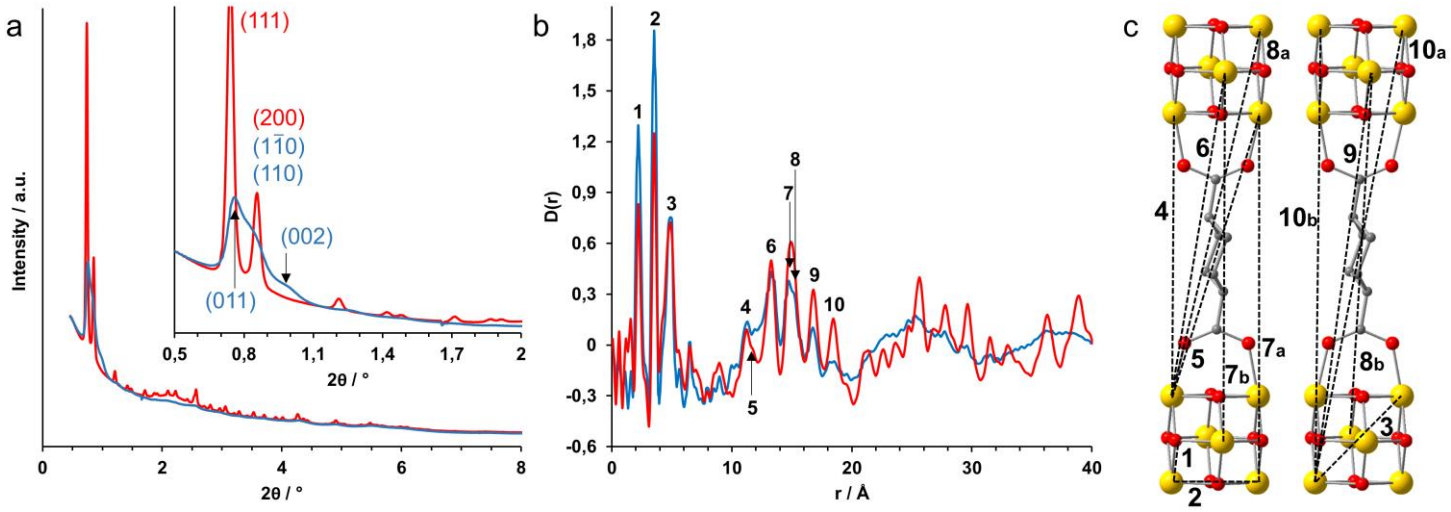

Figure 2 a) Powder X-ray diffraction data (λ=0.1551 Å) and b) pair distribution function D(r) of ethanol-loaded ZrCDC (red trace) and $ZrCDC_{cp}$ (blue trace). Characteristic reflections for each phase are indicated. c) Characteristic Zr<C->Zr distances indicated in the PDF. O red, C gray, Zr yellow.

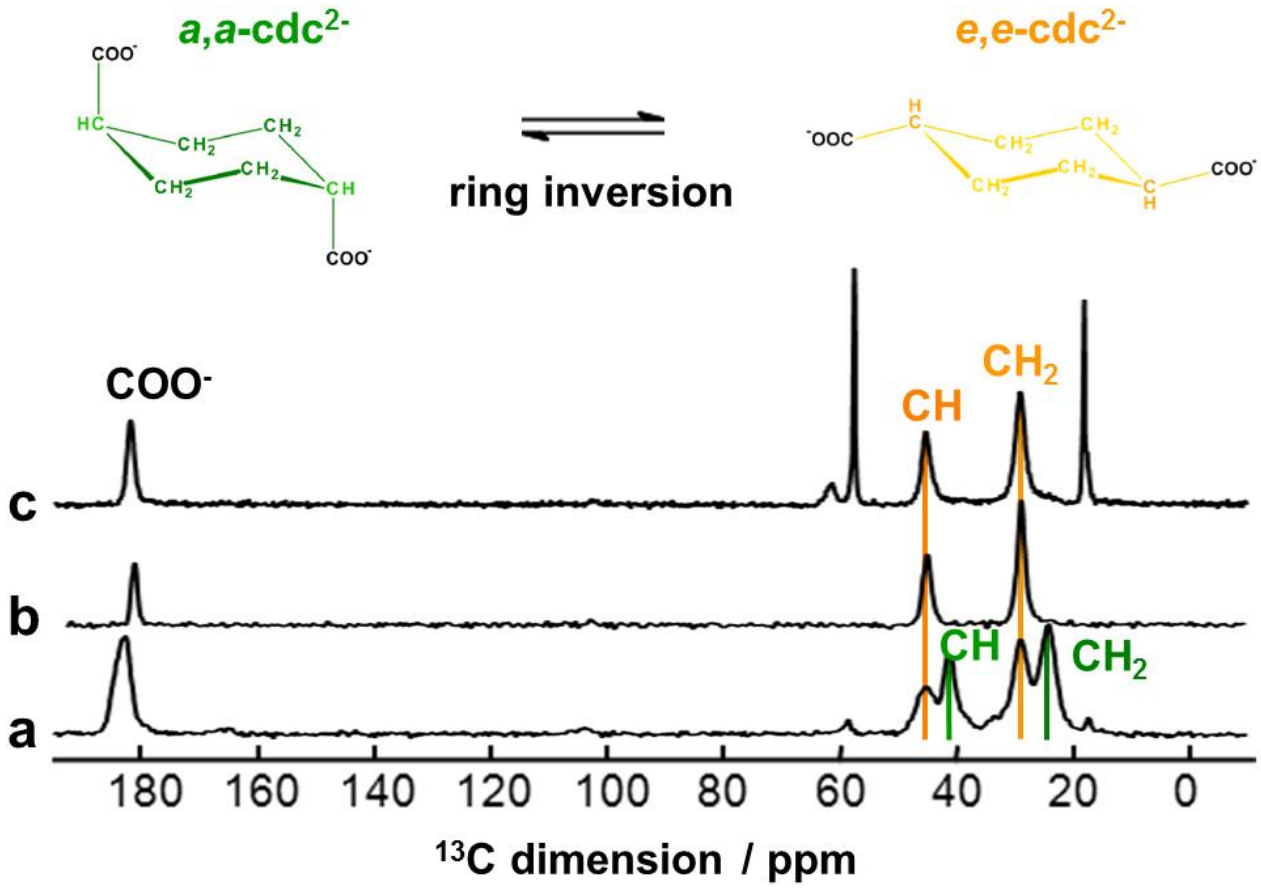

Figure 3 ^{13}C MAS NMR spectra of $ZrCDC_{cp}$ (a), and ZrCDC after water (b) and ethanol adsorption (c). Besides *e*,*e*-cdc^{2-} (CH_2=29.0 ppm, CH=45.8 ppm), $ZrCDC_{cp}$ also contains *a*,*a*-cdc^{2-} (CH_2=24.3 ppm, CH=41.5 ppm) in a maximal ratio of 2:1 to *e*,*e*-cdc^{2-}. Ethanol CH_3 18.1 ppm, CH_2 57.8 ppm.

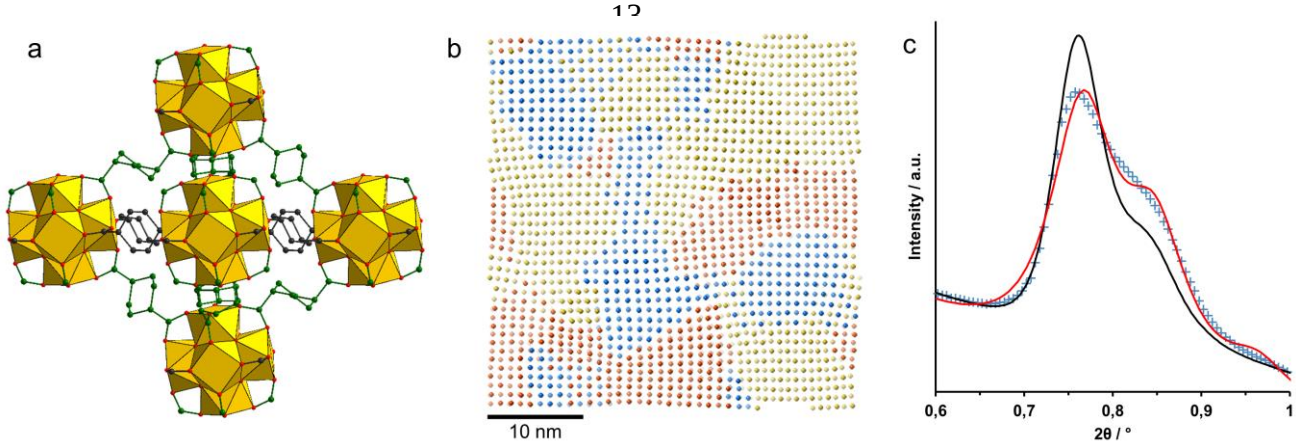

Figure 4 Model of $ZrCDC_{cp}$. a) Contraction of two thirds of the linkers (green) results in a tetragonally distorted cell. O red, C black/green, Zr yellow. b) Cluster growth model simulation. Contraction along the three cubic <100> directions yields randomly oriented, short-range ordered tetragonal nanodomains. Dots represent inorganic nodes, colors indicate domains of different orientations. c) Diffraction pattern for this nodal model (black trace), experimental diffraction pattern of $ZrCDC_{cp}$ (blue crosses) and Pawley fit in the tetragonal space group *I*4/*mmm* (red trace; R_{wp}=1.922 %).